Mediators of Inflammation

WILEY

RESEARCH ARTICLE OPEN ACCESS

Imidazole Propionate Induces Kidney Damage by Activating the ROS-NLRP3 Signaling Pathway Through mTOR Inhibition of Autophagy in Renal Tubular Epithelial Cells

Chen Zeng[1] | Yu-Ru Xiao[1,2] | Si-Qing Li[3] | Man Guo[1,4,5] | Qi Wu[1,4,5,6] | Yi-Meng He[1] | Yu-Fan Zhang[1] | Xiao-Zhen Tan[1] | Yong Xu[1,4,5] | Fang-Yuan Teng[1,4,5]

[1]Department of Endocrinology and Metabolism, The Affiliated Hospital of Southwest Medical University, Luzhou 646000, Sichuan, China | [2]Department of Endocrinology and Metabolism, Zigong First People's Hospital, Zigong 643000, Sichuan, China | [3]Department of Orthopedics, The Third Central Hospital of Tianjin, Tianjin 300170, China | [4]Metabolic Vascular Diseases Key Laboratory of Sichuan Province, Metabolic Vascular Diseases Key Laboratory of Sichuan-Chongqing Cooperation, The Affiliated Hospital of Southwest Medical University, Luzhou 646000, Sichuan, China | [5]Sichuan Clinical Research Center for Nephropathy, Sichuan Clinical Research Center for Diabetes and Metabolic Disease, The Affiliated Hospital of Southwest Medical University, Luzhou 646000, Sichuan, China | [6]Department of Pathology, The Affiliated Hospital of Southwest Medical University, Luzhou 646000, Sichuan, China

Correspondence: Yong Xu (xywyll@swmu.edu.cn) | Fang-Yuan Teng (tengfangyuan383@swmu.edu.cn)

Received: 9 July 2025 | **Revised:** 27 January 2026 | **Accepted:** 30 January 2026

Academic Editor: Tânia Silvia Fröde

Keywords: autophagy | human renal tubular epithelial cells | ImP | NLRP3 | ROS

ABSTRACT

L-Histidine, a parent structure of environmental contaminants (e.g., pesticides and preservatives), may undergo bioaccumulation through the food chain and be metabolized by the gut microbiota into deleterious compounds, ultimately compromising human health. Recent studies have identified abnormally elevated levels of the histidine-derived metabolite imidazole propionate (ImP) in the serum of type 2 diabetes mellitus patients. However, the pathophysiological implications of excessive ImP on renal function and its underlying molecular mechanisms remain poorly characterized. This study is the first to elucidate the detrimental effects of ImP on renal function in mice and its molecular mechanisms. Our findings demonstrate that ImP exacerbates renal dysfunction and induces structural and functional abnormalities in renal tubules. Mechanistically, ImP significantly suppresses autophagy in renal tubular epithelial cells and activates the reactive oxygen species (ROS)-NOD-like receptor pyrin domain-containing 3 (NLRP3) signaling pathway, thereby promoting the expression of the pro-inflammatory cytokine interleukin-1β (IL-1β). Notably, the mechanistic target of rapamycin (mTOR) inhibitor rapamycin (Rap) restores autophagy, inhibits the ROS/NLRP3/IL-1β axis, and mitigates ImP-induced renal injury. Transcriptomic sequencing of mouse kidneys reveals that ImP upregulates the expression of autophagy- and inflammation-related genes, while its inhibitor suppresses these genetic alterations. This study highlights the potential nephrotoxic effects of ImP and underscores the therapeutic value of Rap, providing a theoretical foundation for understanding the role of gut microbiota metabolites in the pathogenesis, prevention, and treatment of kidney diseases.

Chen Zeng and Yu-Ru Xiao and Si-Qing Li contributed equally to this work.

This is an open access article under the terms of the Creative Commons Attribution License, which permits use, distribution and reproduction in any medium, provided the original work is properly cited.

Copyright © 2026 Chen Zeng et al. *Mediators of Inflammation* published by John Wiley & Sons Ltd.

Summary

- Imidazole propionate (ImP) induces renal impairment in mice through upregulation of pro-inflammatory mediators.
- Mechanistically, ImP activates mechanistic target of rapamycin (mTOR) signaling, suppresses autophagy in renal tubular epithelial cells, and culminates in reactive oxygen species (ROS) generation and NOD-like receptor pyrin domain-containing 3 (NLRP3) inflammasome activation, thereby mediating renal injury.
- The mTOR inhibitor rapamycin (Rap) can effectively inhibit the renal injury induced by ImP.

1 | Introduction

Histidine, an essential amino acid, exhibits multifaceted biological significance owing to its distinctive imidazole ring structure. This molecular feature enables its critical involvement in proton buffering, metal ion chelation, scavenging of rreactive oxygen species/reactive nitrogen species (ROS/RNS), erythropoiesis, and modulation of histaminergic signaling pathways [1]. Studies have shown that imidazole compounds are closely linked to environmental pollution, including benzimidazole-based corrosion inhibitors, imidazole fungicides (e.g., Imazalil), and imidazole herbicides (e.g., clotrimazole and ketoconazole) [2–4]. Many common foods, such as meat and dairy products, are now found to contain imidazole derivatives, which may pose potential health risks to humans [5, 6].

It is noteworthy that histidine is closely associated with dysbiosis of the human gut microbiota and can be catabolized by gut bacteria into Imidazole propionate (ImP)—a novel metabolite. ImP was initially reported to exhibit strong associations with tumor development in type 2 diabetes patients, progression of cardiovascular diseases, and metabolic disorders [7]. Subsequent studies have confirmed that in the pathological state of diabetes, ImP impairs insulin receptor substrate (IRS)-mediated insulin signaling by activating the p38γ MAPK signaling pathway, promoting p62 phosphorylation, and subsequently activating the mechanistic target of rapamycin (mTOR) complex 1 (mTORC1). However, ImP exhibits markedly divergent biological effects in different disease contexts: in multiple studies involving tumor diseases such as prostate cancer and glioblastoma, ImP exerts antitumor effects by inhibiting the nuclear factor kappa-B (NF-κB) signaling pathway, thereby delaying disease progression [8–10]. ImP can independently predict major adverse cardiovascular events (MACEs) in patients with atherosclerosis, irrespective of traditional risk factors, primarily by inducing atherosclerosis via the imidazoline-1 receptor (I1R, also known as nischarin) in myeloid cells [11, 12]. Within the nervous system, ImP can enter the bloodstream, reach the brain, induce alterations in the gene expression of hypothalamic neurons, and disrupt GABAergic/Glutama-tergic signaling pathways, thereby leading to hypothalamic dysfunction accompanied by stress-related behaviors [13]. Serum ImP levels and the ImP-histidine ratio are positively correlated with incident type 2 diabetes (T2D), and in the diabetic pathological state, ImP activates the p38γ MAPK signaling pathway, impairs IRS-mediated insulin signaling, and promotes p62 phosphorylation to subsequently activate mTORC1 [14, 15].

Based on the above research background, this study aims to investigate the effects and mechanisms of ImP on the kidneys of normal mice. Through the establishment of in vivo and in vitro experimental models, we found that exogenous ImP can cause renal tubular dysfunction and induce renal inflammatory responses. These research findings not only reveal the biological effects of ImP under normal physiological conditions but also suggest that it may serve as a novel biomarker for early kidney disease, providing a new theoretical basis for early warning and intervention of kidney diseases.

2 | Results

2.1 | Effects of ImP on the Renal Function of Normal Mice

To explore the potential effects of ImP on the renal function of normal mice, referring to the drug concentrations reported in the literature [14, 16, 17], the experimental C57BL/6 mice were randomly divided into three groups, with six mice in each group: the ImP group (100 μg, intraperitoneal injection), the ImP combined with Rap (3 mg/kg) intervention group, and the normal saline control group (NC). The experimental results showed that compared with the NC group, the body weight of the mice in the ImP group increased significantly ($p < 0.05$), while the body weight decreased significantly after the combined Rap intervention ($p < 0.05$) (Figure 1A), but there was no significant difference in the fasting blood glucose levels among the groups (Figure 1B).

To further evaluate the renal function, we detected the urinary albumin/creatinine ratio (ACR). The results showed that the ACR level in the mice of the ImP group increased significantly, and the Rap intervention could effectively reverse this trend (Figure 1C). The pathological findings further explained the changes in ACR levels. Histopathological analysis showed that in the mice of the ImP group, the glomerular basement membrane was thickened, the mesangial matrix proliferated with cell proliferation, and there were also pathological changes such as renal tubular hypertrophy and hyperplasia (Figure 1D). Thickening of the glomerular basement membrane, together with mesangial matrix proliferation accompanied by cellular hyperplasia, can impair the function of the filtration barrier, and thus increase albumin leakage. In contrast, hypertrophy and hyperplasia of renal tubules reduce albumin reabsorption due to structural and functional abnormalities of tubular epithelial cells. These two aspects jointly contribute to the elevation of ACR levels [18, 19]. Rap intervention significantly ameliorated the ImP-induced renal pathological damage and reduced the ACR levels.

To clarify the renal inflammatory response induced by ImP, we detected the expression level of interleukin-1β (IL-1β) in the renal tissues by immunohistochemistry. The results showed that the expression of IL-1β in the renal tubules of the ImP group was significantly upregulated, and the Rap intervention could effectively inhibit its expression (Figure 1E). In addition, the change trend of the serum IL-1β level was consistent with the tissue expression results (Figure 1F). The above results indicate that ImP can cause renal function damage in normal mice and induce renal tubular inflammatory response, while Rap can effectively alleviate this pathological process.

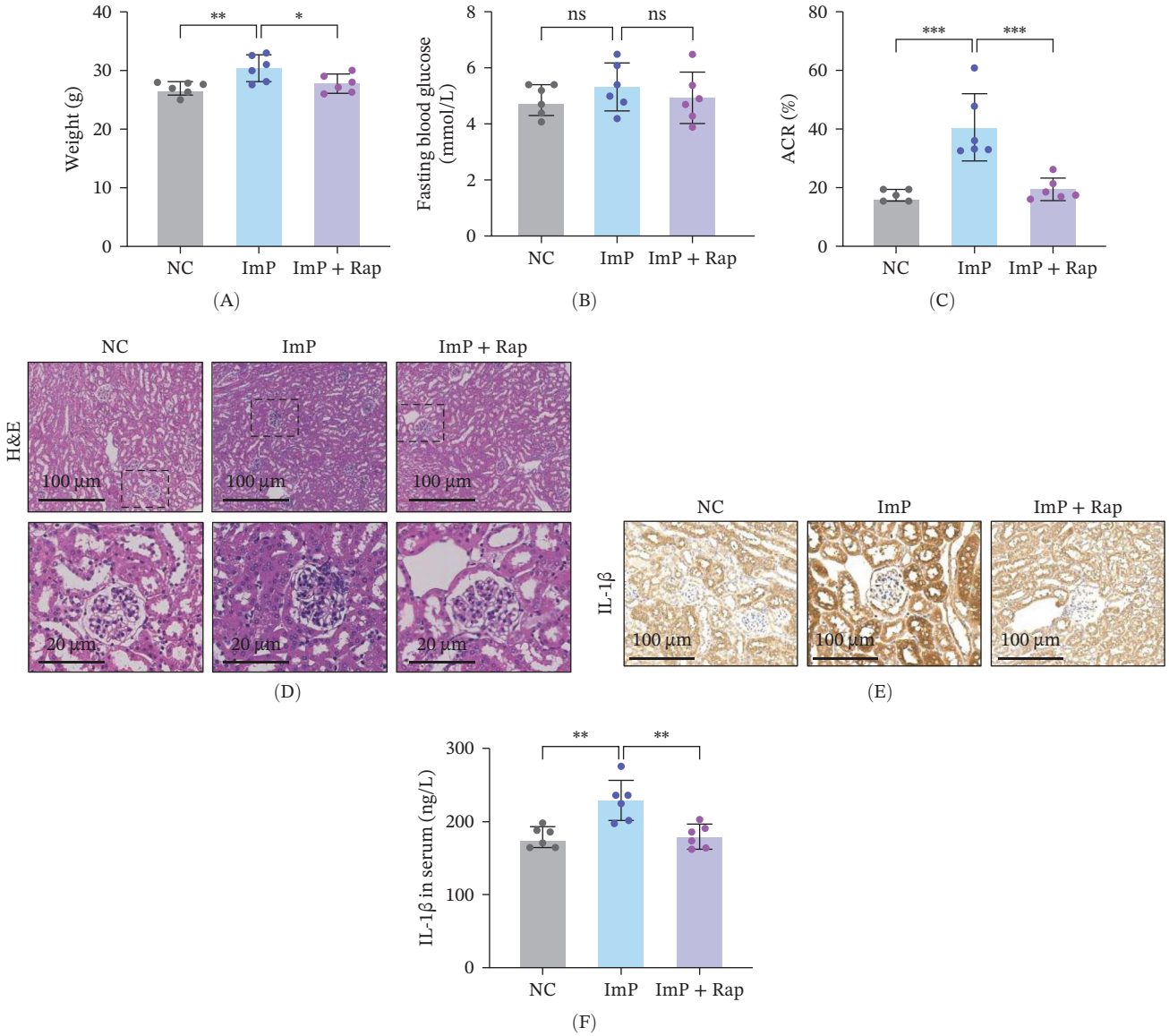


FIGURE 1 | Effects of ImP on the renal function of normal Mice. (A) Following a 3-month intraperitoneal administration of ImP and ImP + Rapamycin (Rap) to mice, body weight, (B) fasting blood glucose, and (C) albumin-to-creatinine ratio (ACR) were monitored and statistically analyzed ($n = 6$). (D) Hematoxylin and eosin (H&E) staining was performed on tissue samples, (E) followed by immunohistochemical (IHC) analysis to assess IL-1β expression. (F) Serum IL-1β levels were quantified via enzyme-linked immunosorbent assay (ELISA) (*, $p < 0.05$; **, $p < 0.005$; ***, $p < 0.0005$).

2.2 | Effects of ImP and Rap on the Autophagy level of Renal Cells in Vitro and in Vivo

Based on previous studies, this study treated human renal tubular epithelial cells (HK-2) with three concentrations of ImP (ImP1, ImP2, and ImP3 respectively correspond to 50, 100, and 200 μmol/L) to investigate its effect on renal cell proliferation [16]. The results showed that ImP significantly inhibited HK-2 cell proliferation in a concentration-dependent manner after 24 and 48 h of treatment ($p < 0.05$; Figure 2A, B). Meanwhile, the expression levels of cell cycle regulatory proteins—cyclin D1 (CYCLIN D1) and cyclin-dependent kinase 2 (CDK2)—were gradually downregulated with increasing concentrations of ImP ($p < 0.05$; Figure 2C, D). Animal experiments also confirmed that ImP significantly reduced the expression of CYCLIN D1 and CDK2 in renal tissues, while Rap intervention effectively reversed the downregulation of these proteins ($p < 0.05$; Figure 2E, F). The results were consistent in cell experiments ($p < 0.05$; Figure 2G, H). According to literature reports, the physiological activity levels of the mTOR and AMPK pathways in renal tissue are crucial for maintaining renal cell growth and differentiation, structural integrity, and normal renal function [20]. Therefore, we first detected the expression levels of key molecules in the mTOR signaling pathway in the renal tissues of mice. The results of Western blot showed that compared with the NC group, the expression of phosphorylated mTOR (p-mTOR) proteins in the ImP group was significantly upregulated ($p < 0.05$; Figure 2I, J), while there were no significant differences in the expression levels of phosphorylated AMPK (p-AMPK)/AMPK and phosphorylated AKT (p-AKT)/AKT (Figure 2K). To further validate this result, we conducted parallel experiments in the HK-2 cell model. The results showed that ImP intervention could activate the mTOR signaling pathway in a dose-dependent manner (Figure 2L, M), and Rap intervention could significantly reverse this effect (Figure 2O, P). Consistent with the animal experiments, there

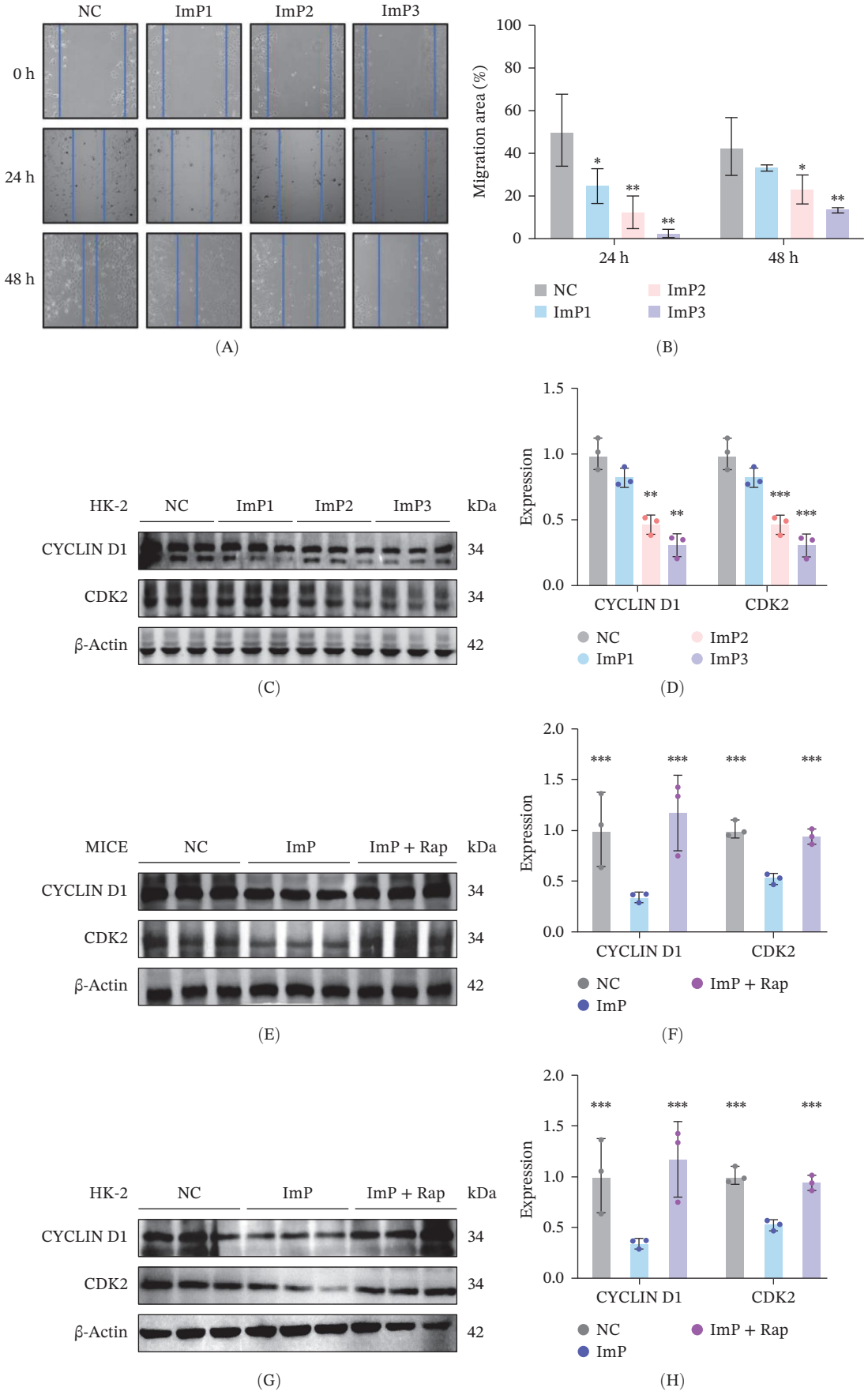


FIGURE 2 | (Continued)

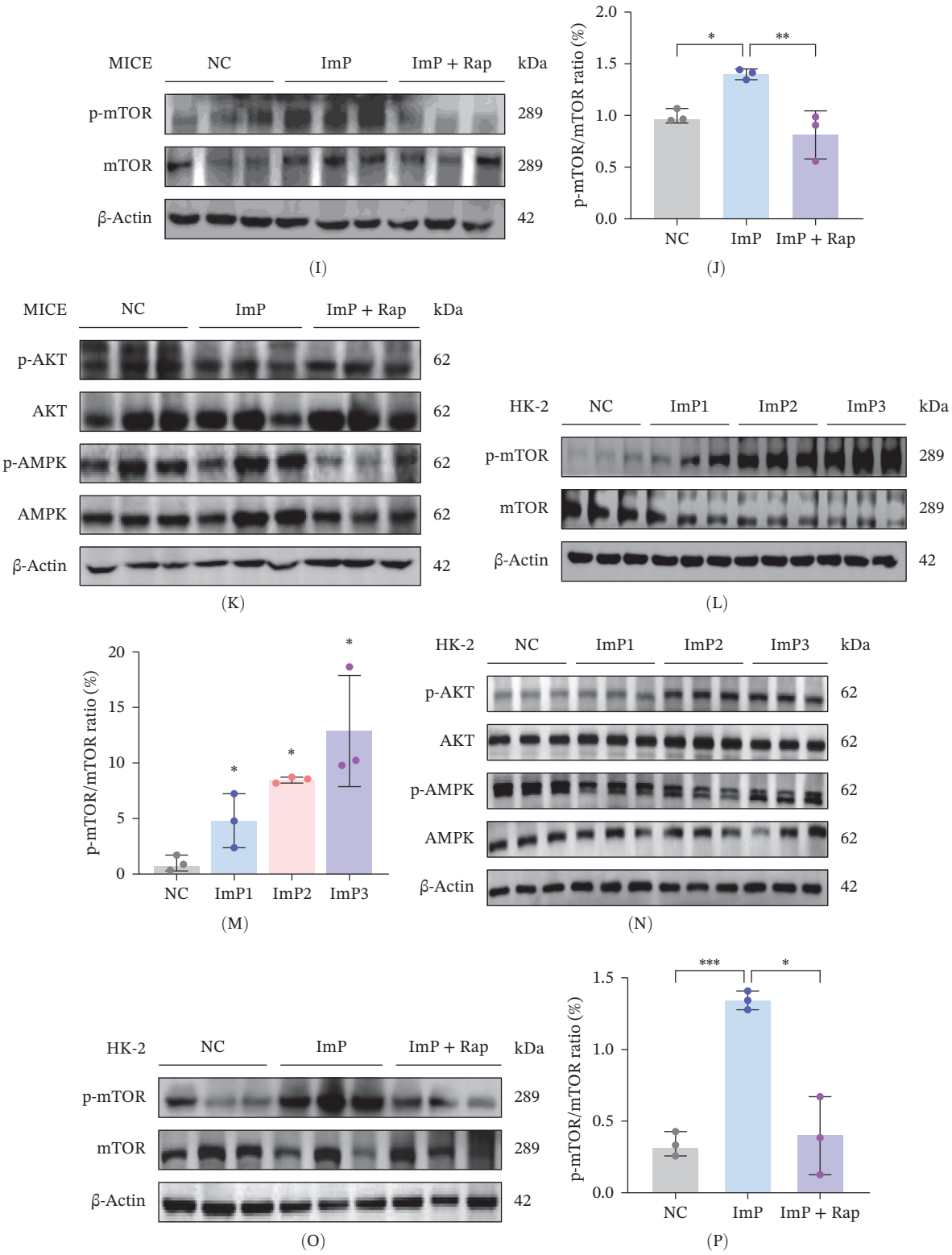


FIGURE 2 | (Continued)

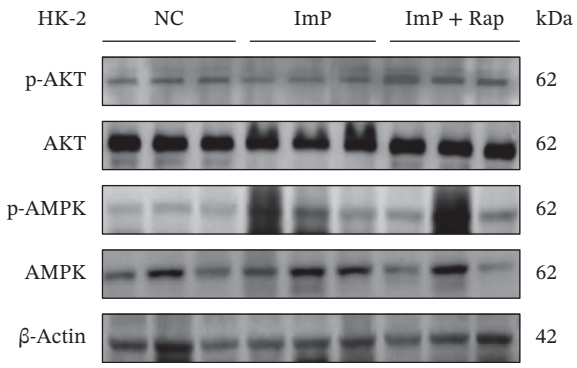


FIGURE 2 | Effects of ImP and Rap on the autophagy level of renal cells in vitro and in vivo. (A,B) Cell migration (as determined by scratch assay) was evaluated at 24 and 48 h post-ImP treatment; ImP1, ImP2, and ImP3 respectively correspond to 50, 100, and 200 μmol/L. (C,D) The protein levels of CYCLIN D1 and CDK2 in HK-2 cells were measured after ImP exposure. (E–H) Subsequently, after treatment with rapamycin (Rap) in both animal and cellular models, we determined the expression levels of the aforementioned proteins in renal tissues and renal cells. (I,J) Western blot analysis was performed to assess the expression of mTOR, phosphorylated mTOR (p-mTOR) in mice treated with ImP or ImP + Rap. (K) AKT, AMPK, p-AKT and p-AMPK in mice treated with ImP or ImP + Rap. (L–N) The protein expression levels of the aforementioned markers were examined in HK-2 cells exposed to a concentration gradient of ImP. (O–Q) Protein expression of these markers was further evaluated in HK-2 cells treated with ImP alone or ImP + Rap. (*, $p<0.05$; **, $p<0.005$; ***, $p<0.0005$).

was still no difference in the protein expression of p-AMPK/AMPK and p-AKT/AKT after HK-2 intervention (Figure 2N, Q). These results indicate that ImP can specifically activate the mTOR signaling pathway.

2.3 | Effects of ImP and Rap on Autophagy Levels in Renal Cells In Vivo and In Vitro

Given the central role of mTOR in autophagy regulation, we further investigated whether autophagy participates in ImP-mediated renal injury [21]. Microtubule-associated protein 1 light chain 3/Microtubule-associated protein 2 light chain 3 (LC3II/LC3I), a marker of autophagosomes, exhibits expression levels positively correlated with autophagic activity. The results of the animal experiments showed that, compared with the NC group, the expression of LC3II/LC3I protein was significantly decreased while p62 protein levels were markedly increased in the renal tissues of mice in the ImP group ($p<0.05$). Rap intervention substantially restored LC3II/LC3I expression and reduced p62 levels (Figure 3A, B). In vitro experiments revealed that ImP inhibited HK-2 cell autophagy activity in a dose-dependent manner, an effect reversible by Rap treatment ($p<0.05$; Figure 3C,D,F,G). To further validate alterations in autophagic flux, we employed the mRFP-GFP-LC3 dual fluorescent labeling system, which demonstrated that ImP significantly suppressed autophagic flux in a dose-dependent manner (Figure 3E), and Rap restores autophagy (Figure 3H). These findings collectively indicate that ImP inhibits renal cellular autophagy through activation of the mTOR signaling pathway.

2.4 | Effects of ImP and Rap on the ROS-NOD-like receptor pyrin domain-containing 3 (NLRP3) Signaling Pathway in Renal Cells In Vivo and In Vitro

A complex regulatory interplay exists between autophagy and the ROS-NLRP3 signaling pathway. Autophagy not only modulates intracellular ROS levels but also regulates inflammatory responses by influencing NLRP3 inflammasome activation [22]. To elucidate this mechanism, we assessed NLRP3 expression in mouse kidneys via immunohistochemistry, measured intracellular ROS levels using the DCFH-DA fluorescent probe, and analyzed NLRP3, cleaved Caspase-1, and IL-1β protein expression by Western blot. The results demonstrated that compared with the NC group, the ImP group exhibited significantly elevated NLRP3 expression in renal tubules (Figure 4A) and markedly upregulated NLRP3, cleaved Caspase-1, and IL-1β protein levels in renal tissues ($p<0.05$; Figure 4B). Rap intervention significantly reduced NLRP3 expression ($p<0.05$), suppressed ROS generation ($p<0.05$), and inhibited the overexpression of cleaved Caspase-1 and IL-1β ($p<0.05$; Figure 4B).

In cellular experiments, ImP treatment significantly increased ROS levels in HK-2 cells (Figure 4C) and induced dose-dependent upregulation of NLRP3, cleaved Caspase-1, and IL-1β protein expression ($p<0.05$; Figure 4D) compared with the NC group. Rap pretreatment markedly attenuated ROS production ($p<0.05$; Figure 4E) and suppressed the excessive expression of NLRP3, cleaved Caspase-1, and IL-1β proteins ($p<0.05$; Figure 4F). These data collectively suggest that ImP induces renal inflammatory responses via activation of the ROS-NLRP3 signaling pathway, while Rap intervention effectively mitigates this process.

2.5 | mRNA Sequencing and Analysis

Subsequently, we collected renal tissues from mice for RNA sequencing. The PCA plot revealed clear separation among the three groups (Figure 5A). As illustrated in the volcano plot, 3 months of ImP intake resulted in 152 upregulated genes and 24 downregulated genes. Rap treatment led to 29 upregulated and 264 downregulated genes (Figure 5B). A total of 87 overlapping genes were identified among the NC, ImP, and ImP + Rap groups (Figure 5C). To explore the functional classification of these differentially expressed genes (DEGs), functional enrichment analysis was performed. In NC and ImP kidneys, pathways enriched in the ImP group were primarily associated with "signaling

receptor activity" and "molecular transducer activity" (Figure 5D), whereas the NC group showed enrichment in "extracellular matrix structural constituent" and "cytoskeletal protein binding." Compared with the ImP group, the ImP + Rap group exhibited enrichment in "mitochondrial protein–containing complex," "fatty acid catabolic process" and "mitochondrial translation" (Figure 5E). Kyoto Encyclopedia of Genes and Genomes (KEGG) pathway analysis revealed that "metabolic pathways" and "MAPK signaling" were enriched in NC and ImP kidneys (Figure 5G), while the ImP+Rap group showed enrichment in pathways such as "mitophagy" and "proximal tubule bicarbonate reclamation" (Figure 5G).

3 | Discussion

Imidazole compounds, which demonstrate significant bioaccumulation in the food supply, may mediate adverse health outcomes through intestinal microbiota interactions postingestion. The interaction between gut microbiota and kidney diseases constitutes a complex and bidirectional regulatory network, which has become a hot research area in nephrology in recent years. The gut microbiota establishes the gut–kidney axis signaling pathway through its interaction with the host intestinal mucosal system via its metabolites [23]. Under physiological conditions, gut microbiota ferments dietary fiber to produce metabolites such as short-chain fatty acids (SCFAs), bile acids, and tryptophan

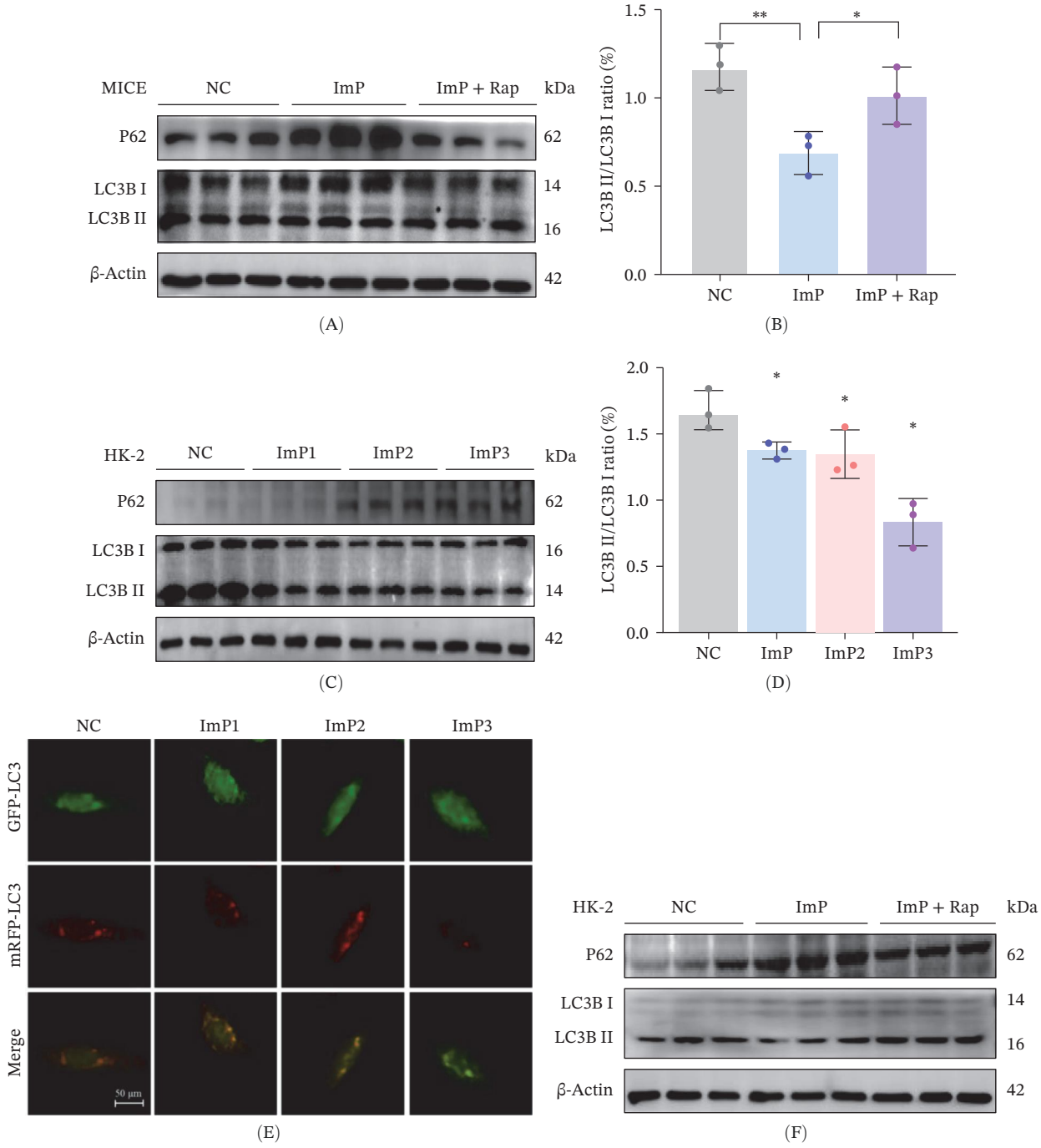


FIGURE 3 | (Continued)

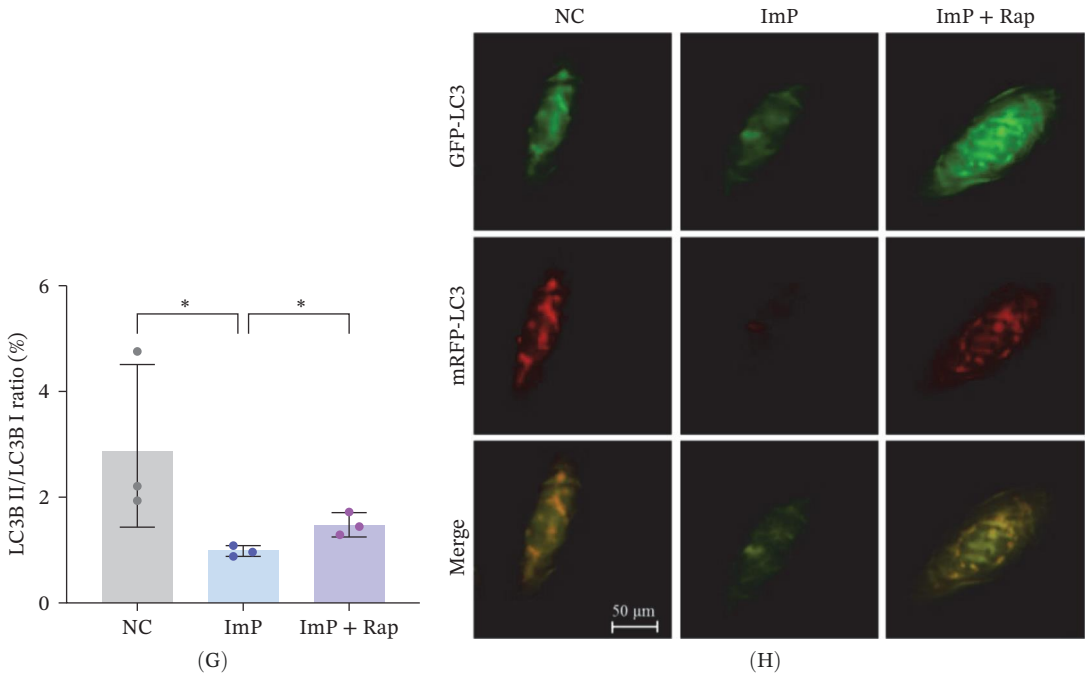


FIGURE 3 | Effects of ImP and Rapamycin on Autophagy Levels in Renal Cells In Vivo and In Vitro. (A,B) Western blot analysis was performed to evaluate the expression of P62 and LC3B II /I in mice treated with ImP or ImP + Rapamycin (Rap). (C,D) The protein levels of P62 and LC3B II /I, (E) along with autophagic flux, were examined in HK-2 cells exposed to gradient concentrations of ImP. (F–H) Expression of these autophagy-related markers and autophagic flux were further assessed in HK-2 cells treated with ImP alone or ImP + Rap (*, $p < 0.05$; **, $p < 0.005$; ***, $p < 0.0005$).

derivatives. These substances have various renal protective effects, including anti-inflammatory, anti-fibrotic, and regulation of lipid metabolism [24, 25]. However, in patients with chronic kidney disease (CKD), the gut microbiota often undergoes significant dysbiosis, manifested by a decrease in beneficial bacteria (such as *Bifidobacterium* and *Lactobacillus*), and the proliferation of opportunistic pathogens (such as *Enterobacteriaceae*). This dysbiosis leads to an increase in the production of uremic toxins (such as indoxyl sulfate and p-cresyl sulfate), which enter the systemic circulation through the portal vein system and ultimately exacerbate kidney damage [26]. Therefore, gut microbiota metabolites may become novel biomarkers for the early diagnosis and prognosis assessment of kidney diseases.

ImP, as the end product of histidine metabolism by gut microbiota, has received increasing attention for its pathophysiological effects. Molinaro et al. found that the levels of ImP in the serum of prediabetic and diabetic patients were significantly elevated, and the fecal microbiota of diabetic patients produced a higher concentration of ImP in an in vitro culture system [27]. An identical finding was also validated in another large-scale clinical study involving patients with diabetes [15]. Animal studies have shown that ImP can promote the phosphorylation of downstream S6K1 by activating the mTOR signaling pathway, accelerate the degradation of insulin IRS, and thus induce insulin resistance and glucose metabolism disorders [28]. In addition, Koh et al. [14] found that ImP can weaken the hypoglycemic effect of metformin by inhibiting the phosphorylation of AMPK [29]. Based on these findings, we speculated that ImP may be involved in disease progression by regulating the mTOR and AMPK signaling pathways. However, the biological effects and mechanisms of ImP in healthy individuals have not been elucidated. Our previous study found that ImP has a concentration-dependent cytotoxic effect on HK-2 cells. Mechanistic studies have shown that ImP stimulation can significantly increase the production of intracellular ROS ($p < 0.05$) and upregulate the protein expression of NLRP3, cleaved Caspase-1, and IL-1β in a dose-dependent manner ($p < 0.05$). Animal experiments further confirmed that ImP intervention can lead to damage to mouse renal tissues and an increase in the levels of serum inflammatory factors, which are highly consistent with the results of cell experiments. These results suggest that ImP may cause kidney damage by activating the ROS-NLRP3 signaling pathway, but its specific molecular mechanism still needs further clarification.

As a central mechanism underlying the pathogenesis and progression of renal diseases, oxidative stress exerts pivotal regulatory effects across multiple renal pathological processes [30–32];. Aberrant accumulation of ROS not only directly induces structural and functional damage to glomerular and tubular cells, but also activates the NF-κB signaling pathway, upregulating the expression of profibrotic mediators such as transforming growth factor-beta (TGF-β), thereby exacerbating renal inflammatory responses and fibrotic progression (17). In disease models including diabetic nephropathy, hypertensive nephropathy, and acute kidney injury, pathological stimuli such as hyperglycemia, angiotensin II, and ischemia-reperfusion significantly enhance ROS generation, while compensatory dysfunction of the antioxidant defense system further amplifies oxidative stress injury [30, 33, 34];. Notably, oxidative stress serves as a critical activation signal for the NLRP3 inflammasome in renal pathophysiology. This multiprotein complex, composed of NLRP3, apoptosis-associated speck-like protein (ASC), and Caspase-1, facilitates the maturation and release of proinflammatory cytokines, including IL-1β and IL-18 through Caspase-1 activation, thereby triggering cascading inflammatory reactions [35];. Substantial evidence demonstrates marked activation of the NLRP3 inflammasome in diverse renal disease models encompassing acute kidney injury, CKD, and immune-mediated renal injury [36–39];.

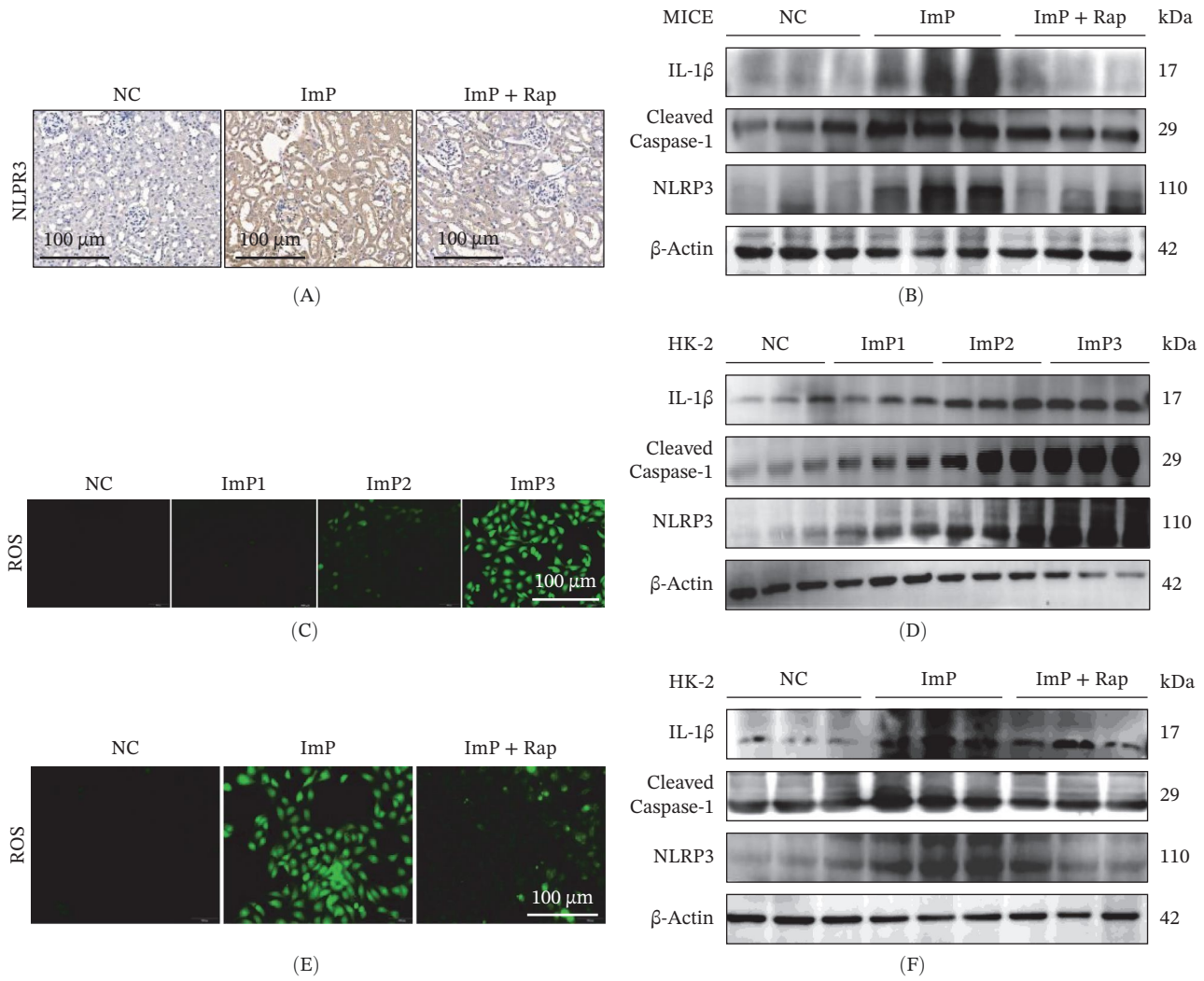


FIGURE 4 | Effects of ImP and Rapamycin (Rap) on the ROS-NLRP3 signaling pathway in Renal Cells in Vivo and in Vitro. (A,B) IHC analysis was performed to assess NLRP3 expression in the control group, ImP-treated mice, and ImP + Rap-treated mice. (C) Protein levels of IL-1β, NLRP3, and cleaved Caspase-1 were further evaluated, (D) along with intracellular reactive oxygen species (ROS) fluorescence. (E) Expression of ROS fluorescence were analyzed in HK-2 cells treated with ImP alone or ImP + Rap. (F) Expression of IL-1β, NLRP3, and cleaved Caspase-1 fluorescence were analyzed in HK-2 cells treated with ImP alone or ImP + Rap (*, $p < 0.05$; **, $p < 0.005$; ***, $p < 0.0005$).

Experimental studies confirm that pharmacological inhibition of NLRP3 inflammasome activation or blockade of the IL-1β signaling pathway significantly attenuates renal inflammation [40], providing a theoretical foundation for targeting the NLRP3/IL-1β axis in nephropathy therapeutics. Mitochondria, as the primary intracellular sites of ROS production, frequently exhibit functional derangements under pathological conditions, leading to excessive ROS generation. Mechanistic studies reveal that ROS-driven NLRP3 inflammasome activation potently enhances IL-1β and IL-18 expression, a process effectively inhibited by ROS scavengers such as Rap Deleted [41];. These findings further validate the critical role of the ROS-NLRP3 inflammasome signaling cascade in renal disease pathogenesis.

In recent years, autophagy has garnered increasing attention in renal pathophysiology as a critical homeostatic mechanism regulating cellular integrity through lysosomal degradation of damaged proteins and organelles, particularly under nutrient deprivation or stress conditions. The autophagic process involves five sequential stages: initiation, nucleation, elongation, maturation, and degradation [42];. This evolutionarily conserved stress-response system plays a pivotal role in cellular maintenance, with dysregulated autophagy being implicated in diverse pathologies including neurodegenerative disorders, metabolic syndromes, and chronic inflammation [43–45]. Nevertheless, the precise mechanistic involvement of autophagy in renal diseases remains incompletely characterized. Of particular interest are the central regulatory roles of the mTOR and AMP-activated protein kinase (AMPK) in coordinating autophagic activity with cellular growth and metabolic processes, warranting deeper investigation into their pathophysiological relevance to CKD progression [46, 47].

Our experimental findings demonstrate through in vivo and in vitro models that ImP exposure induces marked upregulation of IL-1β and NLRP3 expression predominantly localized to renal tubular compartments. Following ImP treatment, dose-dependent inhibition of both proliferation and autophagy was observed in HK-2 cells, accompanied by a significant increase in the levels of phosphorylated mTOR and p62 proteins ($p < 0.05$), while no substantial effects were detected on p-AMPK/AMPK or p-AKT/AKT expression ($p > 0.05$). Notably,

Rap pretreatment effectively reversed ImP-induced mTOR hyperactivation (p-mTOR), restored p62 accumulation, and rescued LC3-II expression deficits ($p < 0.05$). These findings collectively suggest that ImP exerts its nephrotoxic effects through mTOR-mediated suppression of renal tubular autophagy. This mechanistic insight positions mTOR pathway modulation as a potential therapeutic target for counteracting ImP-induced renal damage (Figure 6).

While this study systematically elucidates ImP nephrotoxicity and its underlying molecular pathways, several limitations warrant consideration. First, the investigation did not address potential gut microbiota alterations mediated by ImP, despite established recognition of the gut–kidney axis in disease pathogenesis. Second, the concentration of IMP intervention in this animal experiment was derived from the existing literature [16];. Furthermore, the absence of serum ImP pharmacokinetic profiling limits therapeutic monitoring implications. Future research directions should prioritize: (1) quantitative assessment of ImP levels across renal pathologies (acute kidney injury, CKD, diabetic nephropathy) with correlation analysis between fecal/serum ImP concentrations and disease progression; (2) comprehensive evaluation of ImP-induced gut microbial dysbiosis; (3) identification of specific gut microbiota species regulating ImP metabolism and their therapeutic potential in renal disease modulation. These studies will provide a more reliable basis for clinical prevention and treatment strategies targeting IMP nephropathy.

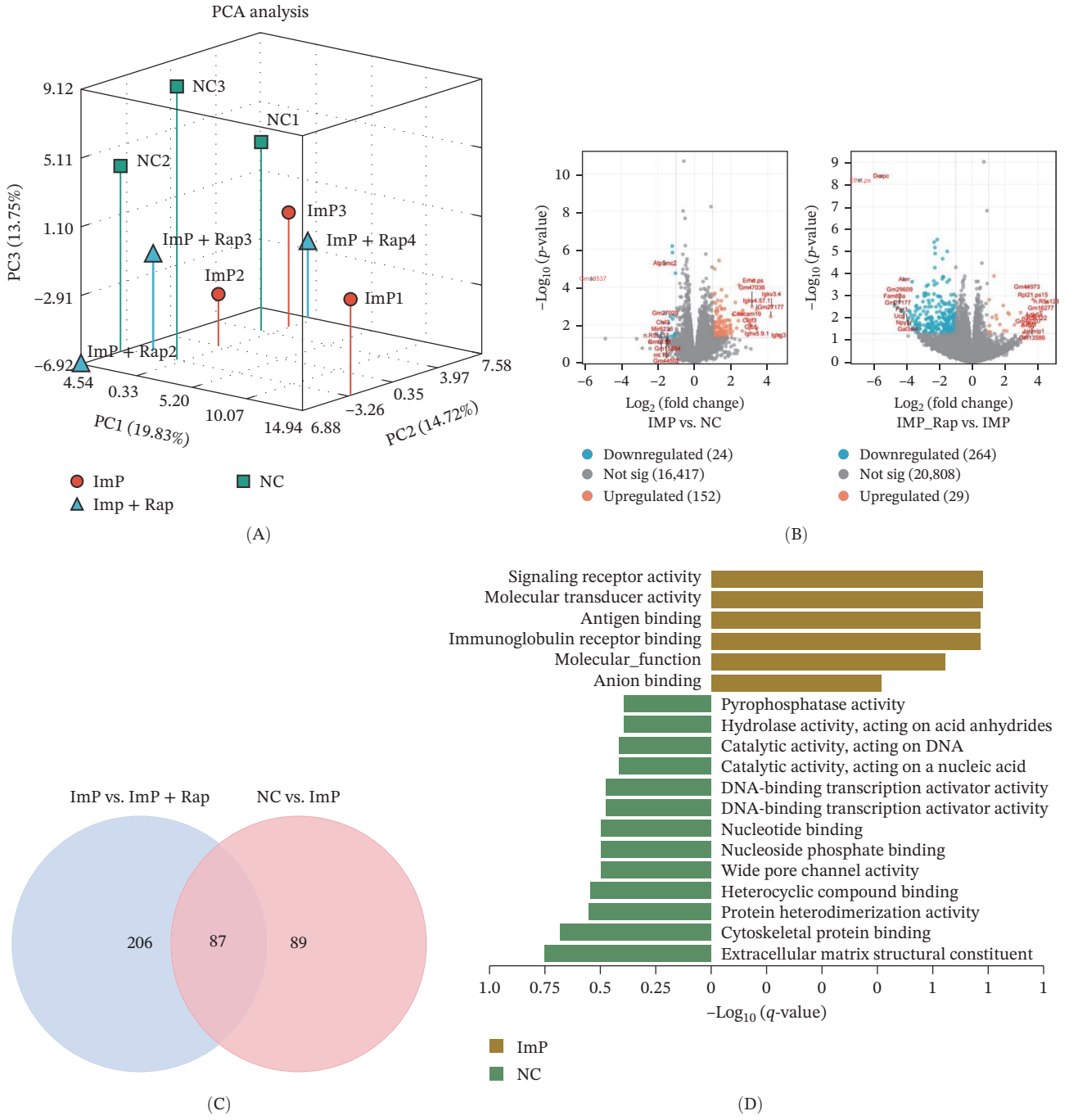
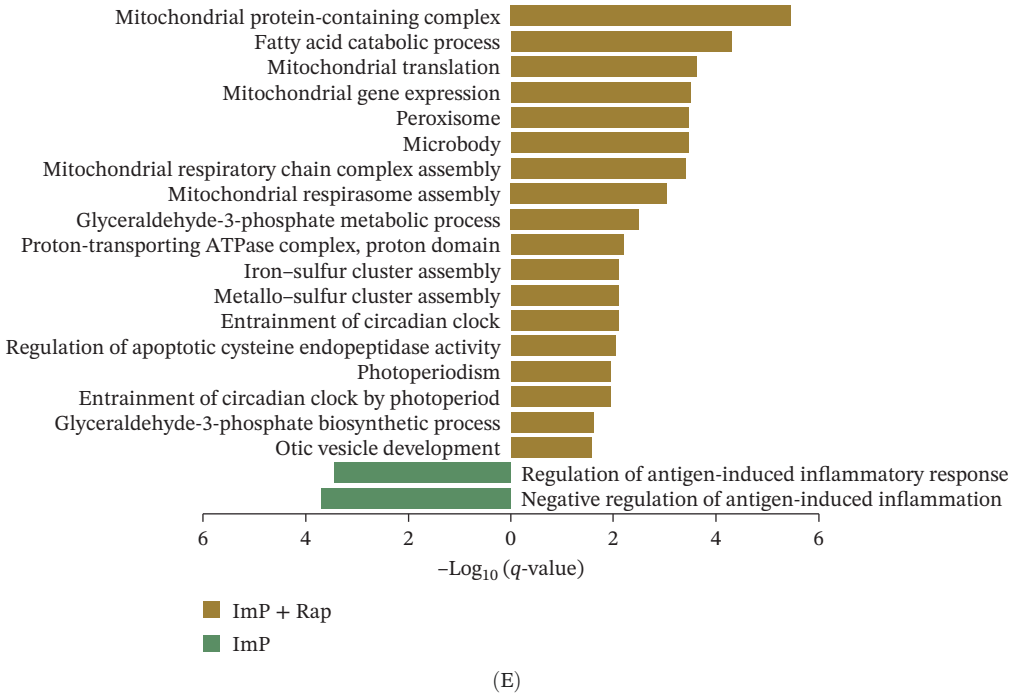
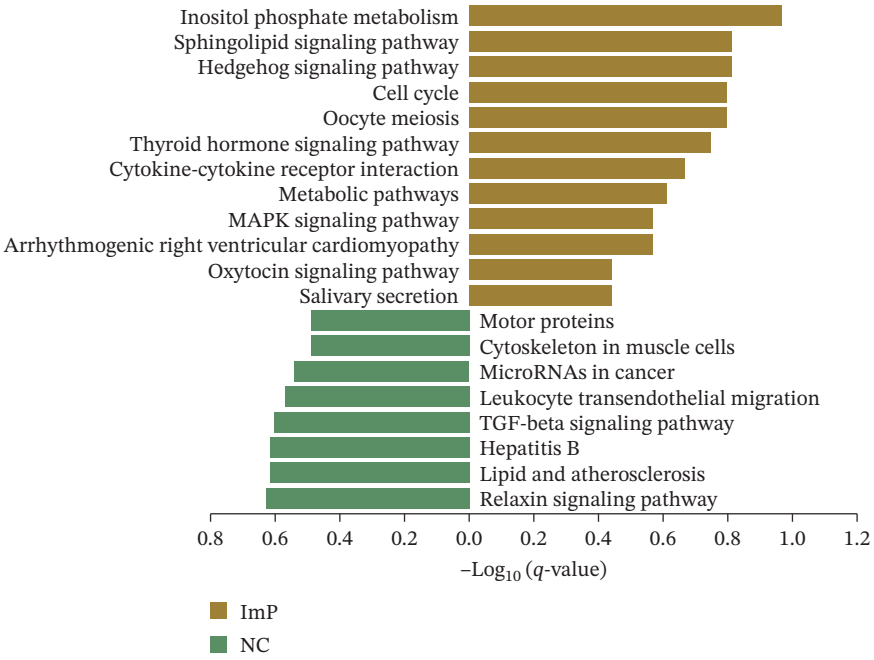


FIGURE 5 | (Continued)



(E)



(F)

FIGURE 5 | (Continued)

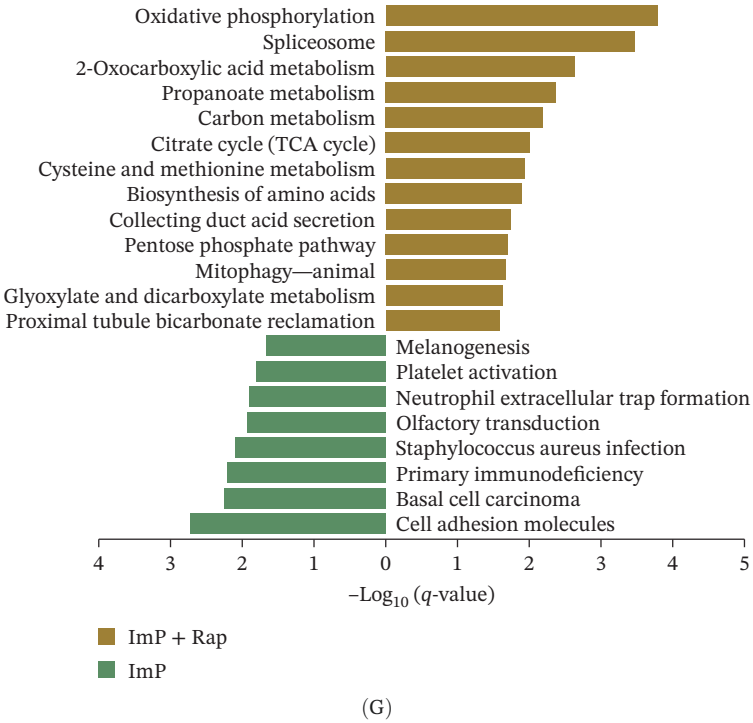


FIGURE 5 | mRNA Sequencing and Analysis. (A) Principal Component Analysis (PCA) plot. (B) Volcano plot. (C) Venn diagram. (D,E) Gene Ontology (GO) enrichment plot. (F,G) Kyoto Encyclopedia of Genes and Genomes (KEGG) pathway enrichment plot.

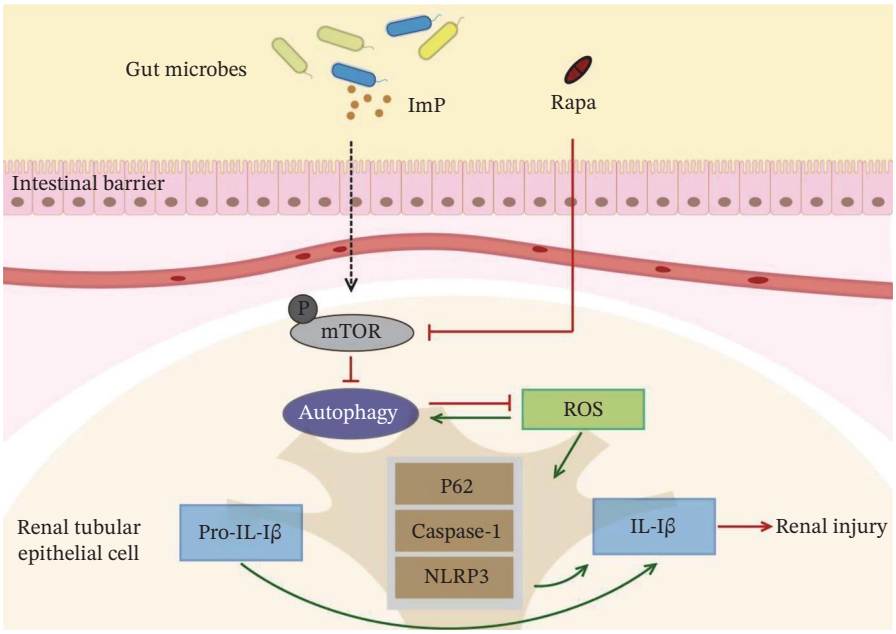


FIGURE 6 | Schematic diagram of the mechanism of ImP.

4 | Materials and Methods

4.1 | Chemicals and Antibodies

The chemicals used in this study include ImP and Rap. The antibodies used include CDK2 Monoclonal antibody, Cyclin D1 Monoclonal antibody, Rabbit anti-human mTOR monoclonal antibody, Rabbit anti-human p-mTOR (phosphorylated mTOR) monoclonal antibody, Rabbit anti-human LC3B monoclonal antibody, Mouse anti-human p62 monoclonal antibody, Rabbit anti-human NLRP3 monoclonal antibody, Rabbit anti-human Caspase-1 polyclonal antibody, and Mouse anti-human IL-1β monoclonal antibody. Other reagents include Human IL-1β ELISA Kit, ROS Assay Kit, Autophagy Dual-Labeling Adenovirus (mRFP-GFP-LC3).

4.2 | Cell Culture

The HK-2 cell line (RRID: CVCL_0302) was obtained from Procell Life Science & Technology Co., Ltd. in 2024. It originates from the renal proximal tubular epithelium of a male *Homo sapiens*.

Authentication by STR profiling showed a 94.55% match with the reference standard in the ExPASy database. The cells were confirmed to be free of cross-contamination and tested negative for mycoplasma prior to experimental use. HK-2 cells were cultured in Dulbecco's Modified Eagle Medium (DMEM)/F-12 (1:1) medium supplemented with 10% fetal bovine serum (FBS) at 37°C in a humidified 5% CO_2 atmosphere. This cell line was selected for study due to its direct derivation from human renal proximal tubule epithelium, which closely replicates physiological metabolic, transport, and injury response.

4.3 | Mice

Male C57BL/6J mice (6 weeks old) were used in this study. They were housed under a 12-h light/dark cycle with *ad libitum* access to food and water. The mice were randomly assigned to three groups ($n = 6$ per group): the Normal group, the ImP group, and the ImP + Rap group. Starting at 7 weeks of age, daily intraperitoneal injections were administered as follows: the Normal group received 150 μL of normal saline; the ImP group received 100 μg of ImP; and the ImP + Rap group received a co-administration of 100 μg ImP and 3 mg/kg Rap. The doses of ImP and Rap were selected based on previous studies [14, 16, 17]. After 12 weeks of continuous intervention, urine samples were collected. The mice were then euthanized, and serum and kidney tissues were harvested and stored at −80°C for subsequent analysis. All animal procedures were approved by the Animal Ethics Committee of Southwest Medical University (Approval Number SWMU20250051).

4.4 | Scratch Wound Healing Assay

A scratch wound healing assay was performed to evaluate cell migration ability. HK-2 cells were seeded in six-well plates and allowed to reach confluence. A uniform scratch was then created using a sterile pipette tip. Cells were treated with different concentrations of ImP, and images of the scratch were captured under a microscope at 0, 24, and 48 h. The changes in scratch width were quantified using ImageJ software, and the cell migration rate was calculated accordingly.

4.5 | Measurement of Intracellular ROS Levels Using 2,7-Dichlorodihydrofluorescein Diacetate (DCFH-DA)

HK-2 cells seeded in six-well plates were serum-starved for 12 h, then treated with ImP for 48 h. After washing with PBS, cells were incubated with 10 μM 2,7-DCFH-DA (2,7-dichlorodihydrofluorescein diacetate) in serum-free DMEM for 30 min at 37°C. Fluorescence intensity was quantified using a fluorescence microscope (excitation/emission: 488/525 nm). Three independent experiments were conducted.

4.6 | Autophagy Flux Analysis via Dual-Fluorescence-Labeled Adenovirus (mRFP-GFP-LC3) in HK-2 Cells

The frozen adenoviral stock (stored at −80°C) was thawed on ice. The original viral solution (1×10^{10} PFU/mL) was diluted to 1×10^{9} PFU/mL using low-glucose DMEM. After thorough mixing by pipetting, the diluted virus was aliquoted into sterile microcentrifuge tubes, labeled, and stored at 4°C for immediate use (avoiding freeze–thaw cycles). Log-phase HK-2 cells (1×10^{5}/mL) were seeded in six-well plates (2 mL/well) and incubated overnight. After PBS washing, cells were infected with adenovirus (MOI = 100) in 1 mL of medium for 4 h, followed by medium replenishment to 2 mL/well and further incubation for 6–8 h. The viral supernatant was discarded, and 2 mL of fresh complete medium was added. After 48 h of incubation, autophagic flux was analyzed by fluorescence microscopy: green puncta represented autophagosomes, red puncta indicated autolysosomes, and merged yellow puncta signified autophagic vacuoles. Images were captured and quantified using ImageJ software (NIH).

4.7 | ELISA

All reagents were first equilibrated to room temperature (25 ± 2°C). Test samples were added to antibody-precoated microplate wells and incubated at 37°C for 30 min for specific antigen binding. After 3–5 washes with PBST buffer, HRP-conjugated detection antibodies were added and reacted at 37°C for 30 min to form sandwich complexes. Following additional washes, TMB substrate was added for color development (15–30 min). Absorbance at 450 nm was measured using a microplate reader, and target concentrations were calculated against a standard curve.

4.8 | Western-Blot

Protein samples were lysed, quantified by BCA assay, and denatured in Laemmli buffer (95°C, 5 min). After SDS-PAGE (10%–12% gels), proteins were transferred to PVDF membranes via semidry transfer. Membranes were blocked with 5% nonfat milk/TBST, then incubated with primary antibodies (4°C, overnight) and HRP-conjugated secondary antibodies. Signals were detected using ECL and imaged (ChemiDoc).

4.9 | Immunohistochemistry

Kidney tissue was fixed in 10% formalin and embedded in paraffin. Immunostaining was performed in 4 μm paraffin sections for antigen retrieval and protein blocking. Antibodies used in this study included NLRP3 and IL-1β. After immunostaining, sections were counterstained with hematoxylin and observed under Fluorescence microscope. Quantification of positive staining signals was measured and expressed as a percentage of area by ImageJ Software (NIH, Bethesda, MD).

4.10 | Principal Component Analysis

Gene expression data (variance-stabilized via DESeq2) underwent PCA using the R *stats* package. Data were centered and scaled prior to dimensionality reduction. The top three principal components (cumulative variance >70%) were visualized via ggplot2, with 95% confidence ellipses. PERMANOVA (vegan::adonis2) assessed group separation significance ($p < 0.05$). Outliers were identified using Mahalanobis distance (>3σ).

4.11 | Differential Gene Expression Analysis

Raw reads were quality-checked (FastQC v0.11.9) and trimmed (Trimmomatic v0.39; Phred <20). HISAT2 (v2.2.1) aligned reads

to GRCh38, with featureCounts (v2.0.3) quantifying genes. DESeq2 (v1.36.0) normalized counts (negative binomial + TMM), while edgeR (v3.40.2) handled unreplicated samples (exactTest). Differential expression required $|\log2FC| \geq 1$ and false discovery rate (FDR) < 0.05 (Wald test). QC included PCA/hierarchical clustering; pathway analysis used KEGG/Gene Ontology (GO, clusterProfiler v4.6.2). All analyses were run in R (v4.2.0) with parameter optimization.

4.12 | Functional Enrichment Analysis

In the functional enrichment analysis of transcriptomic sequencing data, this study adopted a multi-tiered bioinformatics strategy to systematically characterize the biological features of DEGs. First, differential expression analysis was performed using DESeq2 (v1.38.3), with significance thresholds set at $|\log2FoldChange| \geq 1$ and a FDR-adjusted $p < 0.05$. For the identified DEGs, GO annotation and KEGG pathway enrichment analyses were conducted using clusterProfiler (v4.8.1). Significantly enriched terms/pathways were defined by a corrected p-value < 0.05, and an enrichment factor > 1.5. Protein–protein interaction (PPI) networks were reconstructed using the STRING database (v12.0), and core functional modules were identified via the MCODE plugin in Cytoscape (v3.9.1). Visualization of hierarchical clustering heatmaps and enrichment bubble plots was implemented using ggplot2, ensuring that the results were both statistically robust and biologically interpretable.

4.13 | Statistic Analysis

The data presented are SEM ± mean. For statistical analysis, GraphPad Prism 10 and IBM SPSS Statistics Version 22 software were used. For continuous data from two groups, the t-test was used for analysis; while for data from three or more groups, one-way ANOVA or Kruskal–Wallis test was used as appropriate. A p-value less than 0.05 indicates a significant difference. All p-values were two-tailed tests.

Author Contributions

Chen Zeng: investigation, data curation, writing – original draft, writing – review and editing. **Yu-Ru Xiao**: data curation, methodology, software. **Si-Qing Li**: investigation, methodology.**Man Guo and Xiao-Zhen Tan**: software. **Qi Wu**: methodology. **Yi-Meng He**: validation. **Yu-Fan Zhang**: investigation. **Yong Xu**: conceptualization, resources, software, supervision, writing – review and editing. **Fang-Yuan Teng**: conceptualization, funding acquisition, resources, writing – original draft, writing – review and editing.

Acknowledgments

The authors have nothing to report.

Funding

This work was supported by the Natural Science Foundation of China (Grants U22A20286 and 82470854), the Noncommunicable Chronic Diseases-National Scienceand Technology Major Project (Grant 2024ZD0531300), the Sichuan Province Science and Technology Program (Grant 2025ZNSFSC0741), the Luzhou Science and Technology Program (Grant 2025LZXNYDJC27), and the Scientific Research Funding of Southwest Medical University (Grants 2025LCYXZX33 and 2024LCYXZX02).

Ethics Statement

This experiment has Southwest Medical University Ethical Approval (SWMU20250051).

Consent

All the authors have provided their consent for publication of the manuscript.

Conflicts of Interest

The authors declare no conflicts of interest.

Data Availability Statement

The data supporting the findings of this study are available from the corresponding author upon reasonable request.

References

1. H. López-Laguna, E. Voltà-Durán, E. Parladé, A. Villaverde, E. Vázquez, and U. Unzueta, "Insights on the Emerging Biotechnology of Histidine-Rich Peptides," *Biotechnology Advances* 54 (2022): 107817.

2. M. Cycoń, A. Mrozik, and Z. Piotrowska-Seget, "Bioaugmentation as a Strategy for the Remediation of Pesticide-Polluted Soil: A Review," *Chemosphere* 172 (2017): 52–71.

3. Z. Jin, "Muscarine, Imidazole, Oxazole and Thiazole Alkaloids," *Natural Product Reports* 33, no. 11 (2016): 1268–1317.

4. R. Pamanji, T. N. Kumareshan, S. L. Priya, G. Sivan, and J. Selvin, "Exploring the Impact of Antibiotics, Microplastics, Nanoparticles, and Pesticides on Zebrafish gut Microbiomes: Insights into Composition, Interactions, and Health Implications," *Chemosphere* 349 (2024): 140867.

5. A. G. Abril, P. Calo-Mata, T. G. Villa, et al., "High-Resolution Comparative and Quantitative Proteomics of Biogenic-Amine-Producing Bacteria and Virulence Factors Present in Seafood," *Journal of Agricultural and Food Chemistry* 72, no. 8 (2024): 4448–4463.

6. M. Moniente, D. García-Gonzalo, I. Ontañón, R. Pagán, and L. Botello-Morte, "Histamine Accumulation in Dairy Products: Microbial Causes, Techniques for the Detection of Histamine-Producing Microbiota, and Potential Solutions," *Comprehensive Reviews in Food Science and Food Safety* 20, no. 2 (2021): 1481–1523.

7. A. Molinaro, P. Bel Lassen, M. Henricsson, et al., "Imidazole Propionate is Increased in Diabetes and Associated With Dietary Patterns and Altered Microbial Ecology," *Nature Communications* 11: 5881.

8. M. Matsushita, K. Fujita, T. Hayashi, et al., "Gut Microbiota-Derived Short-Chain Fatty Acids Promote Prostate Cancer Growth via IGF1 Signaling," *ancer Research* 81 (2021): 4014–4026.

9. E. C. Seidel, C. Birkemeyer, R. Baran-Schmidt, J. Meixensberger, H. Oppermann, and F. Gaunitz, "Viability of Glioblastoma Cells and Fibroblasts in the Presence of Imidazole-Containing Compounds," *International Journal of Molecular Sciences* 23, no. 10 (2022): 5834.

10. W. Zhong, K. Wu, Z. Long, et al., "Gut Dysbiosis Promotes Prostate Cancer Progression and Docetaxel Resistance via Activating NF-κB-IL6-STAT3 Axis," *Microbiome* 10, no. 1 (2022): 94.

11. A. Mastrangelo, I. Robles-Vera, D. Mañanes, et al., "Imidazole Propionate Is a Driver and Therapeutic Target in Atherosclerosis," *Nature* 645, no. 8079 (2025): 254–261.

12. F. A. Wenzl, P. Wang, F. Kahles, et al., "Gut Microbiota-Derived Imidazole Propionate Predicts Cardiometabolic Risk in Patients With Coronary Artery Disease." *European Heart Journal* (2025).

13. G. Agirman, M. N. B. Quicho, K. K. Connelley, et al., "The Microbial Metabolite Imidazole Propionate Modulates Hypothalamic Activity and Stress-Induced Behaviors," *Cell Host & Microbe* 33, no. 12 (2025): 2030–2042.e9.

14. A. Koh, A. Molinaro, M. Ståhlman, et al., "Microbially Produced Imidazole Propionate Impairs Insulin Signaling Through mTORC1," *Cell* 175, no. 4 (2018): 947–961.e17.

15. H. Yang, K. Luo, B. A. Peters, et al., "Diet, Gut Microbiota, and Histidine Metabolism Toward Imidazole Propionate Production in Relation to Type 2 Diabetes," *Diabetes Care* 48, no. 7 (2025): 1225–1232.

16. A. Koh, L. Mannerås-Holm, N. O. Yunn, et al., "Microbial Imidazole Propionate Affects Responses to Metformin Through p38γ-Dependent Inhibitory AMPK Phosphorylation," *Cell Metabolism* 32, no. 4 (2020): 643–653.e4.

17. W. Chen, P. Zou, Z. Zhao, et al., "Synergistic Antitumor Activity of Rapamycin and EF24 via Increasing ROS for the Treatment of Gastric Cancer," *Redox Biology* 10 (2016): 78–89.

18. J. R. Ingelfinger, T. Benzing, and D. Salant, "Insights into Glomerular Filtration and Albuminuria," *New England Journal of Medicine* 384, no. 15 (2021): 1437–1446.

19. B.-C. Liu, T.-T. Tang, L.-L. Lv, and H.-Y. Lan, "Renal Tubule Injury: A Driving Force Toward Chronic Kidney Disease," *Kidney International* 93, no. 3 (2018): 568–579.

20. A. González, M. N. Hall, S.-C. Lin, and D. G. Hardie, "AMPK and TOR: The Yin and Yang of Cellular Nutrient Sensing and Growth Control," *Cell Metabolism* 31, no. 3 (2020): 472–492.

21. C. Peña-Martinez, A. D. Rickman, and B. L. Heckmann, "Beyond Autophagy: LC3-Associated Phagocytosis and Endocytosis," *Science Advances* 8, no. 43 (2022): 1702.

22. R.-Q. Yao, C. Ren, Z.-F. Xia, and Y.-M. Yao, "Organelle-Specific Autophagy in Inflammatory Diseases: A Potential Therapeutic Target Underlying the Quality Control of Multiple Organelles," *Autophagy* 17, no. 2 (2021): 385–401.

23. T. Yang, E. M. Richards, C. J. Pepine, and M. K. Raizada, "The Gut Microbiota and the Brain-Gut-Kidney Axis in Hypertension and Chronic Kidney Disease," *Nature Reviews Nephrology* 14, no. 7 (2018): 442–456.

24. R. J. F. Felizardo, I. K. M. Watanabe, P. Dardi, L. V. Rossoni, and N. O. S. Câmara, "The Interplay among Gut Microbiota, Hypertension and Kidney Diseases: The Role of Short-Chain Fatty Acids," *Pharmacological Research* 141 (2019): 366–377.

25. J. J. Liu, J. Ching, H. N. Wee, et al., "Plasma Tryptophan-Kynurenine Pathway Metabolites and Risk for Progression to End-Stage Kidney Disease in Patients With Type 2 Diabetes," *Diabetes Care* 46, no. 12 (2023): 2223–2231.

26. X. Wang, S. Yang, S. Li, et al., "Aberrant Gut Microbiota Alters Host Metabolome and Impacts Renal Failure in Humans and Rodents," *Gut* 69, no. 12 (2020): 2131–2142.

27. Y. C. Kim and K.-L. Guan, "mTOR: a pharmacologic target for autophagy regulation," *Journal of Clinical Investigation* 125, no. 1 (2015): 25–32.

28. L. Fang, Y. Zhou, H. Cao, et al., "Autophagy Attenuates Diabetic Glomerular Damage through Protection of Hyperglycemia-Induced Podocyte Injury," *PLoS ONE* 8, no. 4 (2013): e60546.

29. M. Kajiwara and S. Masuda, "Role of mTOR Inhibitors in Kidney Disease," *International Journal of Molecular Sciences* 17, no. 6 (2016): 975.

30. S. Kishi, H. Nagasu, K. Kidokoro, and N. Kashihara, "Oxidative Stress and the Role of Redox Signalling in Chronic Kidney Disease," *Nature Reviews Nephrology* 20, no. 2 (2024): 101–119.

31. Y. Liu, W. Chen, C. Li, et al., "DsbA-L Interacting With Catalase in Peroxisome Improves Tubular Oxidative Damage in Diabetic Nephropathy," *Redox Biology* 66 (2023): 102855.

32. H. Liu, L. Wang, X. Weng, et al., "Inhibition of Brd4 Alleviates Renal Ischemia/Reperfusion Injury-Induced Apoptosis and Endoplasmic Reticulum Stress by Blocking FoxO4-Mediated Oxidative Stress," *Redox Biology* 24 (2019): 101195.

33. L. L. Camargo, F. J. Rios, A. C. Montezano, and R. M. Touyz, "Reactive oxygen species in hypertension," *Nature Reviews Cardiology* 22, no. 1 (2025): 20–37.

34. J. Wen, Y. Shu, and W. Zhang, "P53, and Ischemic Acute Kidney Injury in Diabetic Models," *Kidney International* 88, no. 1 (2015): 198-199.

35. J. Fu and H. Wu, "Structural Mechanisms of NLRP3 Inflammasome Assembly and Activation," *Annual Review of Immunology* 41, no. 1 (2023): 301–316.

36. X. Dai, R. Liao, C. Liu, et al., "Epigenetic Regulation of TXNIP-Mediated Oxidative Stress and NLRP3 Inflammasome Activation Contributes to SAHH Inhibition-Aggravated Diabetic Nephropathy," *Redox Biology* 45 (2021): 102033.

37. J. Zhong, W. Gong, L. Lu, et al., "Irbesartan Ameliorates Hyperlipidemia and Liver Steatosis in Type 2 Diabetic db/db Mice via Stimulating PPAR-γ, AMPK/Akt/mTOR Signaling and Autophagy," *International Immunopharmacology* 42 (2017): 176–184.

38. K. Shahzad, S. Fatima, H. Khawaja, et al., "Podocyte-Specific Nlrp3 Inflammasome Activation Promotes Diabetic Kidney Disease," *Kidney International* 102, no. 4 (2022): 766–779.

39. Y. L. Chou, H. L. Chen, B. G. Hsu, et al., "Galectin-3 Contributes to Pathogenesis of IgA Nephropathy," *Kidney International* 106, no. 4 (2024): 658–670.

40. Y. Jin, S. Liu, Q. Ma, D. Xiao, and L. Chen, "Berberine Enhances the AMPK Activation and Autophagy and Mitigates High Glucose-Induced Apoptosis of Mouse Podocytes," *European Journal of Pharmacology* 794 (2017): 106–114.

41. W.-J. Ni, L.-Q. Tang, and W. Wei, "Research Progress in Signalling Pathway in Diabetic Nephropathy," *Diabetes/Metabolism Research and Reviews* 31, no. 3 (2015): 221–233.

42. B. Hartleben, M. Gödel, C. Meyer-Schwesinger, et al., "Autophagy Influences Glomerular Disease Susceptibility and Maintains Podocyte Homeostasis in Aging Mice," *Journal of Clinical Investigation* 120, no. 4 (2010): 1084–1096.

43. H. H. Parving, H. Lambers-Heerspink, and D. Zeeuw, "Empagliflozin and Progression of Kidney Disease in Type 2 Diabetes," *The New England Journal of Medicine* 375, no. 18 (2016): 1800-1801.

44. R. A. Nixon and D. C. Rubinsztein, "Mechanisms of Autophagy–Lysosome Dysfunction in Neurodegenerative Diseases," *Nature Reviews Molecular Cell Biology* 25, no. 11 (2024): 926–946.

45. M. Kitada and D. Koya, "Autophagy in Metabolic Disease and Ageing," *Nature Reviews Endocrinology* 17, no. 11 (2021): 647–661.

46. Y. I. Koh, K. S. Oh, J. A. Kim, et al., "OSBPL2 Mutations Impair Autophagy and Lead to Hearing Loss, Potentially Remedied by Rapamycin," *Autophagy* 18, no. 11 (2022): 2593–2614.

47. C. Miao, Y. Shen, Y. Lang, et al., "Biomimetic Nanoparticles with Enhanced Rapamycin Delivery for Autism Spectrum Disorder Treatment via Autophagy Activation and Oxidative Stress Modulation," *Theranostics* 14, no. 11 (2024): 4375–4392.